

Non-resonant two-photon x-ray absorption in Cu

J. J. Kas and J. J. Rehr*

Dept. of Physics, Univ. of Washington Seattle, WA 98195

J. Stöhr

SLAC National Accelerator Laboratory, Menlo Park, CA 94025

J. Vinson

Material Measurement Laboratory, National Institute of Standards and Technology, Gaithersburg, Maryland, 20899

(Dated: July 11, 2025)

We present a real-space Green’s function theory and calculations of two-photon x-ray absorption (TPA). Our focus is on non-resonant K -shell TPA in metallic Cu, which has been observed experimentally at intense x-ray free electron laser (XFEL) sources. The theory is based on an independent-particle Green’s function treatment of the Kramers-Heisenberg equation and an approximation for the sum over non-resonant intermediate states in terms of a static quadrupole transition operator. XFEL effects are modeled by a partially depleted d -band. This approach is shown to give results for K -shell TPA in quantitative agreement with XFEL experiment and with a Bethe-Salpeter Equation approach. We also briefly discuss many-body corrections and TPA sum-rules.

Keywords: Green’s function, Two-photon absorption, XAS, XFEL

I. INTRODUCTION

Two-photon absorption (TPA) and emission (TPE) processes were originally predicted theoretically by Maria Goeppert-Mayer in her doctoral dissertation.^{1,2} However, TPA was not observed until lasers became available and then only for optical frequencies.³ More recently, TPA of hard x-rays has been observed for metallic Cu using intense x-ray free electron laser (XFEL) sources.⁴ Formally, the theory of TPA is based on a sum of amplitudes for two successive dipole transitions over all possible intermediate states. This sum is given by the Kramers-Heisenberg (KH) equation. Energy is conserved only for the net transition, with the transition energy equal to the sum of the two photon energies.^{1,5–7} This process is illustrated by the Feynman diagrams⁸ in Fig. 1. The left diagram depicts a process in which the first photon excites an occupied p -state to the final s - or d -photoelectron state and the second photon excites the $1s$ electron to the now empty p -state. The right diagram depicts the other

possible process, in which the first photon excites the $1s$ electron to an unoccupied p -photoelectron state, and the second photon scatters this photoelectron to the final s - or d -photoelectron state. While the KH approach is tractable for atomic systems,^{5,6} and non-linear approaches have been developed for optical spectra,⁹ quantitative TPA calculations are computationally challenging for condensed matter. However, for K -shell TPA in Cu with ≈ 4500 eV photons,⁴ only non-resonant intermediate states are possible, greatly simplifying the theory. For this case an approximation for K -shell TPA based on the Bethe-Salpeter Equation (BSE) has been proposed.¹⁰

Our goal here is to develop a real-space Green’s function (RSGF) approach for deep core TPA in condensed matter that only includes non-resonant contributions and is applicable for simulations of XFEL spectra. We show that this method can be expressed in a form analogous to one-photon (OPA) x-ray absorption spectra (XAS), but with an effective static quadrupole transition operator. TPA calculations are presented based on an extension of the RSGF XAS code FEFF10.¹¹ XFEL effects on the near-edge are modeled by a partially depleted d -band. This theory yields K -shell TPA spectra for Cu in good agreement with XFEL experiment⁴ and with the BSE approach.⁶

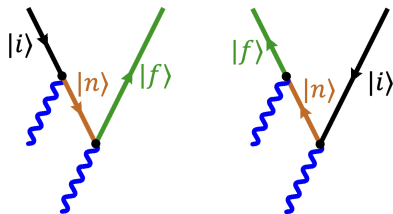


FIG. 1. Feynman diagrams⁸ for the TPA amplitude: Incident photons are represented by wavy lines (blue), the single particle state $|i\rangle$ by the black line, the photoelectron $|f\rangle$ by the green line, and intermediate states $|n\rangle$ by the orange line. The left diagram indicates occupied intermediate states, while the right diagram indicates unoccupied intermediate states.

II. TPA THEORY

Within 2nd-order perturbation theory in the electron-photon interaction, the TPA cross-section σ_{XAS}^{2P} is given

by the many-body Kramers-Heisenberg (KH) equation^{6,7}

$$\sigma_{\text{XAS}}^{2P}(\omega) = 8\pi^3\alpha^2\omega^2 \times \sum_F |M_{IF}(\omega)|^2 \delta_{\Gamma_F}(2\omega + E_I - E_F), \quad (1)$$

$$M_{IF}(\omega) = \sum_X \frac{\langle F|\hat{d}|X\rangle\langle X|\hat{d}|I\rangle}{\omega + E_I - E_X + i\Gamma_X}. \quad (2)$$

Here $|I\rangle$ and $|F\rangle$ denote the initial and final N -electron states of the system with energies E_I and E_F respectively; α is the fine structure constant; $\hat{d} = \sum_i d_i$ is the many-body dipole operator in position-space, where $d_i = \mathbf{r} \cdot \hat{\epsilon}$ is the interaction with monochromatic photons of energy ω and polarization $\hat{\epsilon}$; $|X\rangle$ represent intermediate states with energies E_X ; and the energy denominator $\omega + E_I - E_X + i\Gamma_X$ includes a lifetime broadening Γ_X . Finally, $\delta_{\Gamma_F}(E)$ denotes a Lorentzian with broadening Γ_F associated with the final state lifetime. Unless otherwise specified we use atomic units (a.u.) $e = \hbar = m = 1$, with energies in Hartrees, distances in Bohr $a_0 = 0.529 \text{ \AA}$, and time in atomic units 24.2 as/Hartree.

The derivation of TPA theory is similar to other applications of the KH equation, such as photon-photon scattering,⁸ with analogous Feynman diagrams. Likewise, contributions from the \mathbf{A}^2 term (i.e., the square of the vector potential) in the electron-photon interaction known as the *seagull* diagram,⁸ are ignored since they are arguably of negligible importance.¹² While typically expressed in terms of dipole operators in position-space $\mathbf{r} \cdot \hat{\epsilon}$, the formulation with momentum-space $\mathbf{p} \cdot \hat{\epsilon}$ operators is similar, apart from the ω^2 prefactor in Eq. (1).¹³ In general both resonant intermediate states, where the energy denominator vanishes apart from a lifetime broadening Γ_X , and non-resonant intermediate states, where the energy denominator is non-zero, must be considered. When present, resonant states typically dominate, and interference between resonant and non-resonant terms may also be necessary.

For K -shell TPA for example, $|I\rangle \approx |1s, N-1\rangle$ represents the initial state prior to x-ray absorption where unless otherwise specified, the configuration of the $N-1$ passive electrons is implicit, and in this work also reflects XFEL excitation effects on the system. The final states of interest $|F\rangle = |\overline{1s} kL\rangle$ have a $1s$ hole (denoted with an overline) and a photoelectron with wave number k , energy ϵ_k , and orbital angular momentum quantum numbers $L = (l, m)$. For simplicity we ignore spin indices as well as the differences between $p_{1/2}$ and $p_{3/2}$ spectra; however, these effects are included implicitly in our numerical calculations. Dipole selection rules $l \rightarrow l \pm 1$ then require intermediate states $|X\rangle$ of two types: i) states $|\overline{np}kL\rangle$, with a hole in an np orbital and a photoelectron with d - or s -symmetry; and ii) states $|\overline{1s}kp\rangle$, with a $1s$ core-hole and a virtual photoelectron with p -symmetry. Thus the selection rules for TPA are similar to those of normal quadrupole excitations $\Delta l = 0, \pm 2$, except that $l_i = l_f = 0$ is allowed, and there is an additional restriction $\Delta m = 0$.¹⁴ In the zero-temperature equilibrium

state, near-edge TPA produces photoelectrons in the $3d$ or $4s$ levels above the Fermi energy ϵ_F . Neglecting relaxation of the passive electrons (which is discussed below), the transition energy $E_F - E_I = \epsilon_k - \epsilon_{1s} = 2\omega$. The theory can be extended straightforwardly to other edges.

The RSGF approach is based on an independent-electron approach. Upon integrating over the $N-1$ passive electrons and rearranging terms, the KH expression for the TPA cross-section for a given core-level i can be expressed in terms of single-particle levels, which are denoted with lower-case italic indices

$$\sigma_{\text{XAS}}^{2P}(\omega) = 8\pi^3\alpha^2\omega^2 \times \sum_f^{\text{unocc}} |M_{if}(\omega)|^2 \delta_{\Gamma_i}(2\omega + \epsilon_i - \epsilon_f), \quad (3)$$

$$M_{if}(\omega) = \sum_n \frac{\langle f|d|n\rangle\langle n|d|i\rangle}{\omega + \epsilon_i - \epsilon_n + i\Gamma_n}. \quad (4)$$

Here i and f denote initial-hole and final-photoelectron levels, and $\omega = (\epsilon_f - \epsilon_i)/2$ for photons of equal energy and n ranges over all intermediate states. This relation for the independent particle transition matrix elements M_{if} requires a careful treatment of the various states involved in TPA along with Fermion commutation relations, and is derived in Appendix A, following the approach of Guo.¹⁵ In the independent particle formulation, the two types of intermediate levels n correspond to: 1) occupied levels of the ground state allowed by dipole selection rules when the first photon excites an electron in level n to the photoelectron state f and the second excites an electron in the initial level i to level n , or 2) unoccupied levels allowed by dipole selection rules when the first photon excites an electron in the initial core level i to unoccupied level n and the second scatters that electron to the final level f . These processes are illustrated by the two diagrams Fig. 1. Combining both processes, and assuming that the intermediate state broadening $\Gamma_n \approx \Gamma$ is independent of state n , the sum over intermediate levels n in Eq. (4) is equivalent to the spectral representation of the one-particle Green's function $G(\omega + \epsilon_i)$.¹⁵ Thus the transition matrix can be represented compactly as

$$M_{if}(\omega) = \langle f|dG(\omega + \epsilon_i)d|i\rangle, \quad (5)$$

where $G(\epsilon) \equiv [\epsilon - h + i\Gamma]^{-1}$ and h is the independent-electron Hamiltonian for the intermediate states.

As in OPA, the sum over final states f in Eq. (3) can be treated implicitly using Green's function methods,^{11,16} in terms of the one-particle density matrix

$$\hat{\rho}(\epsilon) \equiv -\frac{1}{\pi} \text{Im} G(\epsilon) \equiv \sum_f |f\rangle\delta(\epsilon - \epsilon_f)\langle f|. \quad (6)$$

Here f are the eigenstates of the final-state independent particle Hamiltonian h' in the presence of the screened core hole. In order to restrict the sum in Eq. (3) to unoccupied levels, a factor $\bar{g}(\epsilon) = 1 - g(\epsilon)$ is appended, that characterizes the distribution. In the ground state $\bar{g}(\epsilon) =$

$\theta(\epsilon_F - \epsilon)$ is just a step function at the Fermi energy. However, in general $\bar{g}(\epsilon)$ is a non-equilibrium distribution¹⁷ that depends on details of the experiment and the x-ray source. For example, in transient XAS studies of warm dense matter (WDM) at fs time-scales the behavior of $g(\epsilon)$ has been addressed using Boltzmann equation methods.¹⁷ At longer ps time-scales, $g(\epsilon)$ is taken to be the Fermi function $f(\epsilon, T) = 1/[\exp((\epsilon - \mu)/k_B T) + 1]$ at the transient electron temperature T in the system, where k_B is the Boltzmann constant.^{18,19} Due to the dependence on depletion, the TPA cross section below the cold edge will not simply be proportional to intensity squared, since the depletion of the occupied orbitals is already proportional to intensity, giving a cubic dependence. The current experimental results were extracted via quadratic fitting analysis, and thus the depletion factor used in our theory can be viewed as an average over the intensities probed in the experiment.

From Eq. (3)-(6) the TPA can be expressed as

$$\sigma_{\text{XAS}}^{2P}(\omega) = 8\pi^3 \alpha^2 \omega^2 \langle i | \tilde{Q}^\dagger(\omega) \tilde{\rho}(\epsilon) \tilde{Q}(\omega) | i \rangle, \quad (7)$$

$$\tilde{Q}(\omega) = d G(\omega + \epsilon_i) d, \quad (8)$$

$$\tilde{\rho}(\epsilon) = \int d\epsilon' A_{\Gamma_i}(\epsilon - \epsilon') \hat{\rho}(\epsilon') \bar{g}(\epsilon'), \quad (9)$$

where $\epsilon = 2\omega + \epsilon_i$, $\tilde{Q}(\omega)$ is a dynamic quadrupole operator, and the convolution over the Lorentzian $A_{\Gamma_f}(\epsilon)$ produces the final state lifetime broadening. This representation of the TPA is valid for both resonant and non-resonant TPA. Thus Green's function methods have been used to calculate TPA both in model and atomic systems.⁵

III. NON-RESONANT TPA

Our primary focus in this work is non-resonant K -shell TPA in Cu with monochromatic linearly polarized photons of energy ω near 4485 eV, as in the XFEL measurements.⁴ To simplify the analysis, we choose polarization $\hat{\epsilon} = \hat{z}$ without loss of generality, as there is no polarization dependence in isotropic systems like Cu. In this case the TPA involves a 2-photon transition from a deep $1s$ level and energy $\epsilon_{1s} \approx -8970$ eV to a photoelectron in level $|f\rangle = |kL\rangle$ with angular momentum indices $L = (l, m)$ for $l = 0$ or 2 , and energy ϵ_k in the unoccupied levels. Due to transient effects of short high intensity XFEL pulses $\bar{g}(\epsilon)$ is a non-equilibrium distribution that characterizes a partially depleted d -band in Cu.¹⁷

For ≈ 4500 eV photons no resonant intermediate states exist for which the energy denominator $D_n(\omega) = \omega + \epsilon_{1s} - \epsilon_n = 0$ in the core-spectrum between the $1s$ level at -8960 eV and ϵ_F . Dipole selection rules imply that the only available intermediate levels n are of p -symmetry with $n \geq 2$, both below and above ϵ_F . At the onset of TPA $2\omega \approx 8970$ eV, and $\omega + \epsilon_{1s} \approx -\omega$. Thus the matrix elements in non-resonant K -edge TPA in Cu depend on

the behavior of the diagonal Green's function elements with angular momentum $l = 1$ at large negative energies $G_1(-\omega) = G_{l=1}(-\omega)$. From its spectral representation, contributions to $G_1(\epsilon)$ from the bound np levels below ϵ_F denoted by $G_1^<(\epsilon)$, can be expressed as a sum over the $2p$ and $3p$ levels. The sum over the p -level continuum above ϵ_F denoted by $G_1^>(\epsilon)$, is less straightforward. However, as argued by Vinson,¹⁰ the energy denominator $D_{np}(\omega) = \omega + \epsilon_{1s} - \epsilon_{np} = \epsilon_f - \epsilon_{np} - \omega$ is nearly constant over several hundred eV for the continuum np levels above ϵ_F , and can be approximated by $D_0 = -\omega$. Then using the projection operator \mathbf{P}_p onto occupied p -levels, the sum can be approximated by

$$G_1^>(-\omega) = \sum_{np>3} \frac{|np\rangle\langle np|}{D_{np}(\omega)} \approx \frac{\mathbf{1} - \mathbf{P}_p}{D_0}, \quad (10)$$

where $\mathbf{1}$ is the unit operator. The error in this approximation is of order $(\epsilon_k - \epsilon_F)/\omega^2$ near ϵ_F , where ϵ_k is the photoelectron energy, and hence is negligible for photoelectron energies ϵ_k near the TPA K -edge in Cu. The approximation in Eq. (10) can be verified by replacing the unit operator with a complete set of one-particle levels and appropriate selection rules. Combining $G_1^<(-\omega)$ from the occupied np levels with $G_1^>(-\omega)$ in Eq. (10). $G_1(-\omega)$ for Cu can be approximated by

$$G_1(-\omega) \approx -\frac{1}{\omega} \left[1 + \sum_{np}^{n=2,3} C_{np} |np\rangle\langle np| \right], \quad (11)$$

where $C_{np} = D_0/D_{np} - 1$. For 4485 eV photons $C_{2p} \approx -4485/(-4485 + 960) - 1 \approx 0.27$, and $C_{3p} \approx -4485/(-4485 + 70) - 1 \approx 0.016$.

From Eq. (7), (8) and (11), the TPA can be expressed in terms of a static quadrupole transition operator Q as

$$\sigma_{\text{XAS}}^{2P}(\omega) = 8\pi^3 \alpha^2 \langle 1s | Q \tilde{\rho}(\epsilon) Q | 1s \rangle, \quad (12)$$

$$Q \equiv d^2 + \sum_{np}^{n=2,3} C_{np} d |np\rangle\langle np| d, \quad (13)$$

where $\epsilon = 2\omega + \epsilon_{1s}$. Note that the factors ω^2 from the matrix elements defined in Eq. (11) cancel the ω^2 prefactor in Eq. (3). This yields,

$$\sigma_{\text{XAS}}^{2P}(\omega) = 8\pi^3 \alpha^2 \sum_L^{l=0,2} |M_L^Q(\epsilon)|^2 \tilde{\rho}_l(\epsilon). \quad (14)$$

Here $M_L^Q(\epsilon) = \langle 1s | Q | kL \rangle$ is the quadrupole transition matrix, and $\tilde{\rho}_l(\epsilon)$ is the l component of the density matrix defined in Eq. (9). The expression in Eq. (14) for non-resonant TPA $\sigma_{\text{XAS}}^{2P}(\omega)$ is a key result of this paper. Analogous effective quadrupole operators have been used in related contexts, e.g., double γ decay in nuclei.²⁰

The treatment of the near-edge TPA with XFEL radiation depends on several factors. At low to intermediate intensities, XFEL effects lead to a partial depletion of the d -band and the emergence of spectra below the cold edge.^{17,21} Although more sophisticated approaches require a Boltzmann equation treatment, for

simplicity here we approximate $\bar{g}(\epsilon)$ by a step function with $\bar{g} = 0.075$ for d -levels below the cold Fermi level and $\bar{g} \approx 1.0$ above, reflecting a broad distribution of the excited $3d$ electrons across high-energy unoccupied states. We also accounted for experimental broadening by adding 1.2 eV to the core-hole lifetime, which is equivalent to Lorentzian broadening. Core-hole screening is also an important consideration. For K -shell TPA in Cu, we find that RSGF calculations that neglect the core-hole potential in the final state are a good approximation, similar to the behavior of $L_{2,3}$ XAS in metals.

For comparison with the RSGF approach outlined in Eqs. (3) – (15), it is useful to compare with the BSE. The key difference is that the BSE uses an electron-hole basis denoted by the composite index $b = \{e, h\}$, where the photo-electron inhabits unoccupied orbitals e and the hole occupied core levels h . However, the BSE also uses the same approximation for the effective quadrupole operator Q in Eq. (13). The BSE analog of Eq. (14) is

$$\sigma^{2P}(\omega) = \frac{8\pi^3\alpha^2}{\Omega N_k} \times \left(-\frac{1}{\pi}\text{Im}\right) \left[\sum_{bb'} \langle i|Q|b\rangle\langle b|\frac{1}{2\omega - H_{\text{BSE}} + i\Gamma}|b'\rangle\langle b'|Q|i\rangle \right]. \quad (15)$$

Here the integral over the Brillouin zone is replaced by a finite sum over N_k points, Ω is the unit cell volume, and the effective BSE particle-hole Hamiltonian is

$$H_{\text{BSE}} = \epsilon_e - \epsilon_h + \sqrt{1 - g(\epsilon_e)}(V_X - W) \sqrt{1 - g(\epsilon_e)}, \quad (16)$$

where ϵ_e and ϵ_h are the energies of the non-interacting electron and hole, V_X is the exchange interaction, W is the direct interaction, and $g(\epsilon)$ is the occupancy of the transient, non-interacting electron states, as discussed in Ref. 10 and 22. Similar to the RSGF approach, the occupation of the upper valence bands (Cu $3d$ and $4s$) was reduced to $g(\epsilon)=0.925$ to account for d -band depletion caused by the XFEL. In Eq. (16) the effect of the core-hole potential and exchange are suppressed as $g(\epsilon) \rightarrow 1$.

IV. CALCULATIONS

Calculations of the TPA using Eq. (14) are carried out using a straightforward extension of the RSGF approach for XAS in FEFF10,^{11,16} by substituting the dipole operator d with Q . As in XAS, the one-particle Green's function for these calculations is based on a quasi-particle approximation that builds in a self-energy and many-body final state effects. That is, $h = h' + \Sigma(\epsilon)$, where h' is the final-state Hartree Hamiltonian in the presence of a screened core-hole, and $\Sigma(\epsilon)$ is the electron self-energy (i.e., the dynamic exchange-correlation potential), which implicitly includes an additional imaginary part representing the $1s$ core-hole lifetime. The Hamiltonian h' implicitly assumes a given electron configuration, in this case that with the partially depleted d -band. The RSGF

calculations are then carried out using spherical muffin-tin potentials.¹⁶ The density matrix at the absorbing atom is represented in terms of the local site-angular momentum scattering-states $R_L(\mathbf{r}, \epsilon)$

$$\rho(\mathbf{r}, \mathbf{r}', \epsilon) = -\frac{1}{\pi}\text{Im} G(\mathbf{r}, \mathbf{r}', \epsilon), \quad (17)$$

$$= \sum_L R_L(\mathbf{r}, \epsilon) R_L^*(\mathbf{r}', \epsilon) \rho_l(\epsilon), \quad (18)$$

where $\rho_l(\epsilon)$ is the local projected density of states for angular momentum l . For convenience in FEFF10, a factor $2k/\pi$ that accounts for spin degeneracy and the density of continuum levels is lumped into the normalization of radial wave-functions.¹⁶ With this convention $\rho_l(\epsilon) = 1 + \chi_l(\epsilon)$, where $\chi_l(\epsilon)$ is the fine-structure for a given angular momentum component l arising from multiple-scattering from neighboring atoms.

The matrix elements $M_L^Q(\epsilon)$ are calculated by first expanding Q , $R_L(\mathbf{r})$, and $R_{1s}(\mathbf{r})$ in spherical harmonics, and integrating over all angles. For a $1s$ initial state, L is that for the photoelectron level $|kL\rangle$. The quadrupole matrix elements $M_L^Q(\epsilon)$ are then given by radial integrals

$$M_L^Q(\epsilon) = q_l \langle R_l(r) | [r^2 R_{1s}(r) + r C_{2p} m_{1s}^{2p} R_{2p}(r) + r C_{3p} m_{1s}^{3p} R_{3p}(r)] \rangle, \quad (19)$$

where $q_l = \langle Y_L^* Y_{10} Y_{10} Y_{00} \rangle$, and $m_{1s}^{np} = \langle R_{np} | r | R_{1s} \rangle$ are radial dipole matrix elements. The terms in Eq. (19) are then calculated using an extension of the non-resonant inelastic scattering (NRIXS) module in the FEFF10 code.²³ Inserting these terms into Eq. (14) then yields all contributions to $|M_L^Q(\epsilon)|^2$ including cross terms. Finally we considered different models for the screened core-hole in K -edge TPA, and found that, similar to L_{23} OPA in metals, to a good approximation the core-hole can simply be ignored. This is done with a *NOHOLE* setting in FEFF10. For comparison we also show results from the BSE approach of Eq. (15), where to account for d -band depletion caused by the XFEL, the occupation of the upper valence bands (Cu $3d$ and $4s$) was reduced to $g(\epsilon) = 0.925$ along with 1.2 eV broadening.

Our RSGF results are presented in Fig. 2. Clearly, the full TPA calculation is in quantitative agreement with experiment, within error bars. The RSGF results are also nearly the same as those with the BSE. This agreement indicates that our approximation of the d -band depletion by a step function is reasonable. Interestingly, all of the contributions to TPA in $|M_L^Q|^2$ including cross-terms are of comparable magnitude. Although the coefficients C_{2p} and C_{3p} are small, these factors are compensated by the matrix elements m_{1s}^{np} that depend on the longer range $2p$ and $3p$ wave-functions.

As a check on the effect of the core-hole, we carried out calculations with a density functional theory (DFT) screened core-hole as in the final state rule (FSR), as shown in Fig. 3. This approximation sharpens the pre-edge peak, and produces a red shift of the peak by ≈ 5 eV, in significant disagreement with experiment.

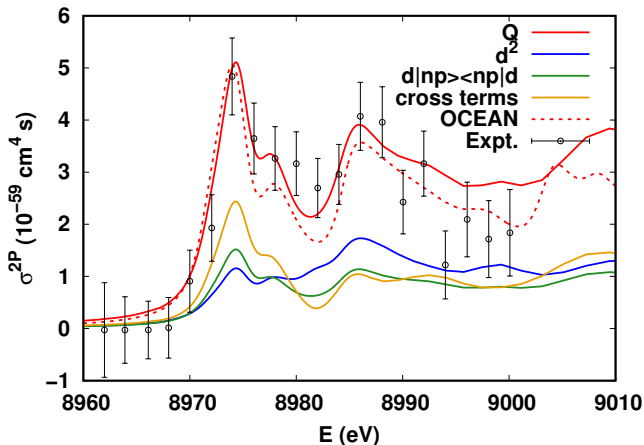


FIG. 2. K -edge two photon absorption spectrum of Cu calculated using RSGF and Eq. (14): full calculation with quadrupole operator Q (red), pure quadrupole operator d^2 (blue), $2p$ and $3p$ contributions (green), cross-terms (gold), and for comparison, results from Eq. (15) using the OCEAN BSE code (red-dashed), and from experiment⁴ (black).

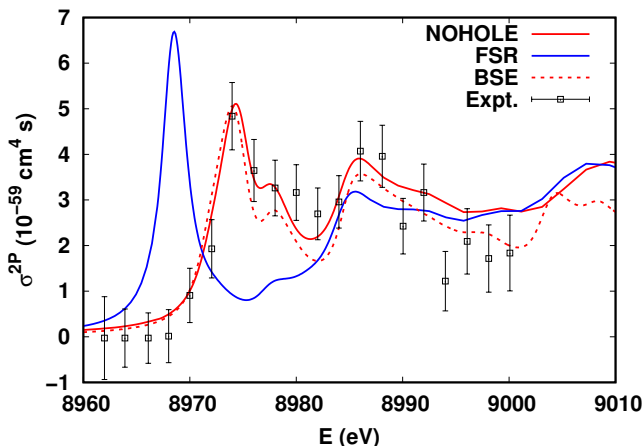


FIG. 3. K -edge two photon absorption spectrum of Cu calculated using RSGF and Eq. (14): full calculation with either no core-hole (red) or a DFT screened full core-hole (FSR) (blue), compared to experiment⁴ (black). and the BSE code OCEAN (red-dashed). Note that FSR screening is too strong and leads to a large unphysical peak below the edge.

We also checked that RSGF calculations of K -edge OPA for Cu using Eq. (13) and similar occupation factors $g(\epsilon)$ have very small contributions from analogous p -band depletion below the cold Fermi level from XFEL sources (Fig. 4). This difference is due to the much smaller p -partial density of states in Cu, consistent with experimental K -edge XFEL OPA for Cu.⁴

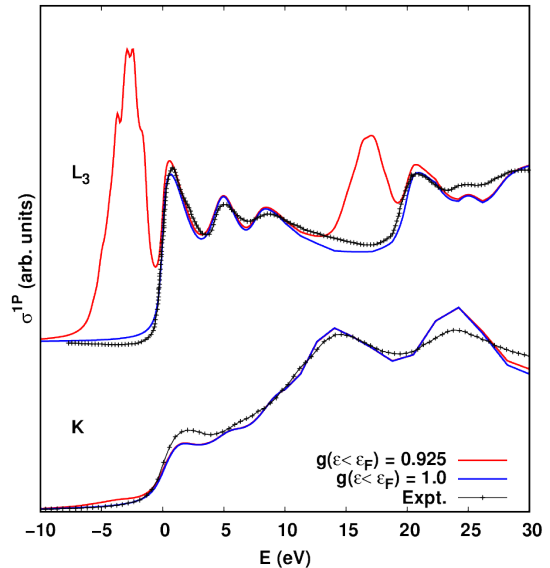


FIG. 4. Cu K -edge (bottom) and L_{23} -edge (top) OPA XANES as a function of energy relative to the cold edge $E = 0$. Calculated results using RSGF with partial occupation (red) and full occupation (blue) of the upper valence states compared to room temperature experimental data (black crosses).²⁴ Note the large effect of partial occupation on the L_{23} -edge compared to the nearly negligible effect on the K -edge.

V. INTERPRETATION AND DISCUSSION

The expressions for the TPA in Eqs. (14) and (15) are formally similar to the golden rule for OPA $\sigma_{\text{XAS}}^{1P}(\omega)$, except for the replacement of the dipole operator d by the quadrupole operator Q

$$\begin{aligned} \sigma_{\text{XAS}}^{1P}(\omega) &= 4\pi^2 \alpha \omega \sum_{kL}^{\text{unocc}} | \langle kL | d | 1s \rangle |^2 \delta_{\Gamma_{1s}}(\omega + \epsilon_{1s} - \epsilon_k) \\ &= 4\pi^2 \alpha \omega \langle 1s | d \tilde{\rho}(\epsilon) d | 1s \rangle, \end{aligned} \quad (21)$$

where $\epsilon = \omega + \epsilon_{1s}$ and $\tilde{\rho}(\epsilon)$ is given by Eq. (9).

Consequently the K -shell TPA in Eq. (14) is formally analogous to L_{23} OPA, i.e.,

$$\sigma_{L_{23}}^{1P}(\omega) = 4\pi^2 \alpha \omega \sum_L^{l=0,2} |M_L(\epsilon)|^2 \tilde{\rho}_l(\epsilon) \quad (22)$$

where $\epsilon = \omega + \epsilon_{2p}$. The main differences are the quadrupole transition operator Q in $|M_L^Q(\epsilon)|^2$ which leads to quadrupole selection rules. The structure of Q has terms from intermediate levels both above and below ϵ_F , corresponding to the contributions from the occupied and unoccupied intermediate states in the Feynman diagrams in Fig. 1. Also, both K -edge TPA and L_{23} XAS have the same s - and d -densities of continuum states $\rho_l(\epsilon)$. However the atomic background from the $2p$ contribution to $|M_L(\epsilon)|^2$ is not identical and the edge

onset is modified in the XFEL experiment due to the d -band depletion, in contrast to ground state calculations.

The expression for $\sigma_K^{2P}(\omega)$ from pure quadrupole contribution d^2 to Q , is related to the K -edge quadrupolar OPA cross-section $\sigma_K^{1P-Q}(\omega_K)$ for photon wave vector $\boldsymbol{\kappa} = (\omega_K/c)\hat{\boldsymbol{\epsilon}}$ at energy $\omega_K = 2\omega$,

$$\sigma_K^{1P-Q}(\omega_K) = 4\pi^2\alpha\omega_K \sum_{L}^{l=0,2} |M_L^{Q_{1P}}(\epsilon)|^2 \tilde{\rho}_l(\epsilon) \quad (23)$$

where $Q_{1P} = i/2(\boldsymbol{\kappa} \cdot \mathbf{r})(\boldsymbol{\epsilon} \cdot \mathbf{r})$, and for K -edge XAS $\omega_K = \epsilon - \epsilon_{1s} = 2\omega$. Comparing Eq. (14) and (23) yields

$$\sigma_K^{2P}(\omega) \approx \frac{2\pi\alpha}{\omega_K\kappa^2} \sigma_K^{1P-Q}(\omega_K) \quad (24)$$

However, there is no contribution to $l = 0$ s -states from Q_{1P} , in contrast to K -shell TPA. In addition, the added weight from the occupied intermediate states in TPA is appreciable.

Though relatively small for Cu, relaxation of the passive $N - 1$ electrons can be important in TPA.⁶ These relaxation effects account for shake-processes, edge singularity effects, and energy shifts due to the sudden turn-on of the $1s$ core-hole. In principle such effects can be added using approximations similar to those for XAS.²⁵ In this approach, the $G(\omega)$ in Eq. (6) is replaced by an effective Green's function $G_{\text{eff}}(\omega) \equiv A * G_{\text{op}}$ that includes a convolution with the core-hole spectral function $A_c(\omega, \omega')$, similar to that for XAS. This spectral function can be approximated, e.g., using cumulant Green's function methods.^{11,25} Moreover, the transition matrix elements must be modified to include a projector onto unoccupied one-particle states of the ground state Hamiltonian h , i.e., $\bar{M}_{if}^Q = \langle 1s|Q\bar{P}|k'L\rangle$, where ϵ'_k are the single-particle energies in the presence of the screened $1s$ core hole. This projector accounts for the Mahan enhancement factor at the edge. Since the effects are not expected to be significant for Cu, the implementation of this extension is reserved for the future.

From Eq. (14), it is straightforward to obtain an approximate sum-rule for the TPA from a given core-level. $\int d\omega \hat{\rho}(2\omega + \epsilon_{1s})\bar{g}(\epsilon) = (1/2)[\bar{\mathbf{P}}(T)] = (1/2)[\mathbf{1} - \mathbf{P}(T)]$, where $\mathbf{1}$ is the unit operator and $\mathbf{P}(T) [\bar{\mathbf{P}}(T)]$ is the projector onto occupied [unoccupied] levels, weighted by $g(\epsilon)$.

$$\int d\omega \sigma_{1s-XAS}^{2P}(\omega) \approx 4\pi^3\alpha^2 \langle 1s|Q\bar{\mathbf{P}}(T)Q^\dagger|1s\rangle \quad (25)$$

$$= 4\pi^3\alpha^2 \left[\langle 1s|QQ^\dagger|1s\rangle - \sum_{nl}^{l=s,d} |\langle 1s|Q|nl\rangle|^2 g(\epsilon_{nl}) \right]. \quad (26)$$

This result reflects the expectation value of QQ^\dagger in a given core-level minus a correction from the projection of Q onto occupied s and d -levels. In contrast, the Thomas-Reiche-Kuhn OPA sum-rule⁸ sums dipole allowed tran-

sitions over all occupied levels,

$$\int d\omega \sigma_{XAS}^{1P}(\omega) = 2\pi^2\alpha \sum_n^{\text{occ}} \langle n|[[h, d], d]|n\rangle = \frac{2\pi^2\alpha\hbar}{m} Z. \quad (27)$$

The prefactor $2\pi^2\alpha\hbar/m$ is independent of the system and has a value $\pi\hbar c r_0 = 0.144 \text{ a.u.} = 110 \text{ Mb eV}$, where $r_0 = e^2/mc^2$ is the classical electron radius.

VI. SUMMARY AND CONCLUSIONS

We have presented a tractable approximation for non-resonant TPA based on an independent particle Green's function treatment of the non-resonant intermediate states, and we have applied it to the K edge of metallic copper. Our formulation starts with the many-body KH formula⁶ and approximates the sum over intermediate states above the Fermi level using a projection onto occupied levels.¹⁰ These closure techniques are similar to those of Stöhr, which assume a constant energy denominator.⁷ These approximations then lead to an expression for non-resonant TPA in Eq. (14) in terms of an effective, static quadrupole operator Q and a non-equilibrium occupancy function $g(\epsilon)$ due to XFEL induced depletion of the valence bands. For K -edge TPA in Cu, Q has only three terms in Eq. (19), a pure quadrupole interaction d^2 and terms from the projectors onto occupied $2p$ and $3p$ states. Our approximation of non-resonant TPA in Eq. (14) is implemented using a straightforward extension of the NRIXS module in the RSGF FEFF10 XAS code. XFEL effects lead to a partially depleted d -band which for simplicity is modeled by a step function distribution $g(\epsilon) = 0.925$ below the cold Fermi level. In addition, we have included 1.2 eV experimental broadening, and a *NOHOLE* approximation. While improved treatments of the distribution function require Boltzmann equation techniques,¹⁷ the present model is already in quantitative agreement with experiment within error bars and in absolute units.⁴ We also find that all contributions including the cross-terms in $|M_L^Q(\epsilon)|^2$ are of comparable magnitude.

Finally an extension of this work for the treatment of two-photon x-ray emission (TPE) is similar in many respects to that for TPA. The difference is analogous to that between XAS and XES,¹⁶ i.e., the main change is the replacement of the complementary distribution function $\bar{g}(\epsilon)$ in Eq. (9) by $g(\epsilon)$ that restricts the initial states to occupied levels.

Acknowledgments — We thank G. Bertsch for illuminating discussions, R. Albers and B. Ziaja for comments, and Alex Kennedy for assistance with some of the calculations. This work is supported in part by the Theory Institute for Materials and Energy Spectroscopy (TIMES) at SLAC, FWP100291 which is funded by DOE Office of Science BSE DMSE Contract DE-AC02-76SF0051. Certain software is identified for informational purposes.

Such identification does not imply recommendation or

endorsement by the National Institute of Standards and Technology.

- * jjr@uw.edu
- ¹ Maria Göppert-Mayer, “Über elementarakte mit zwei quantensprüngen,” *Ann. der Physik* **401**, 273–294 (1931).
 - ² Maria Göppert-Mayer, “Elementary processes with two quantum transitions,” *Ann. der Physik* **18**, 466–479 (2009).
 - ³ W. Kaiser and C. G. B. Garrett, “Two-photon excitation in CaF_2 : Eu^{2+} ,” *Phys. Rev. Lett.* **7**, 229–231 (1961).
 - ⁴ Kenji Tamasaku, Eiji Shigemasa, Yuichi Inubushi, Ichiro Inoue, Taito Osaka, Tetsuo Katayama, Makina Yabashi, Akihiro Koide, Toshihiko Yokoyama, and Tetsuya Ishikawa, “Nonlinear spectroscopy with x-ray two-photon absorption in metallic copper,” *Phys. Rev. Lett.* **121**, 083901 (2018).
 - ⁵ E. J. McGuire, “Two- and three-photon ionization in the noble gases,” *Phys. Rev. A* **24**, 835–848 (1981).
 - ⁶ S. A. Novikov and A. N. Hopersky, “Two-photon excitation/ionization of atomic inner shells,” *J. Phys. B: Atomic, Molecular and Optical Physics* **33**, 2287 (2000).
 - ⁷ Joachim Stöhr, *The Nature of X-Rays and Their Interactions with Matter* (Springer, 2023).
 - ⁸ J. J. Sakurai, *Advanced Quantum Mechanics* (Addison-Wesley Publishing Co., 1967).
 - ⁹ Royce K Lam, SL Raj, TA Pascal, CD Pemmaraju, L Foglia, A Simoncig, Nicola Fabris, P Miotti, CJ Hull, AM Rizzuto, *et al.*, “Soft x-ray second harmonic generation as an interfacial probe,” *Phys Rev Lett* **120**, 023901 (2018).
 - ¹⁰ John Vinson, “Advances in the ocean-3 spectroscopy package,” *Phys. Chem. Chem. Phys.* **24**, 12787–12803 (2022).
 - ¹¹ Joshua J Kas, Fernando D Vila, Tun S Tan, and John J Rehr, “Ab initio calculation of x-ray and related core-level spectroscopies: Green’s function approaches,” *Phys. Chem. Chem. Phys.* **24**, 13461–13473 (2022).
 - ¹² Kenji Tamasaku, Eiji Shigemasa, Yuichi Inubushi, Tetsuo Katayama, Kei Sawada, Hirokatsu Yumoto, Haruhiko Ohashi, Hidekazu Mimura, Makina Yabashi, Kazuto Yamachi, *et al.*, “X-ray two-photon absorption competing against single and sequential multiphoton processes,” *Nature Photonics* **8**, 313–316 (2014).
 - ¹³ Barry Honig and Joshua Jortner, “Theoretical studies of two-photon absorption processes. ii. model calculations,” *J. Chem. Phys.* **47**, 3698–3703 (1967).
 - ¹⁴ Keith D Bonin and Thomas J McIlrath, “Two-photon electric-dipole selection rules,” *J. Opt. Soc. Am. B* **1**, 52–55 (1984).
 - ¹⁵ Dong-Sheng Guo, “Theory of two-photon emission from atomic inner shells,” *Phys. Rev. A* **36**, 4267–4271 (1987).
 - ¹⁶ Alexei L Ankudinov, Bruce Ravel, JJ Rehr, and SD Conradson, “Real-space multiple-scattering calculation and interpretation of x-ray-absorption near-edge structure,” *Phys. Rev. B* **58**, 7565 (1998).
 - ¹⁷ Laurent Mercadier, Andrei Benediktovitch, Špela Krušič, Joshua J Kas, Justine Schlappa, Marcus Agäker, Robert Carley, Giuseppe Fazio, Natalia Gerasimova, Young Yong Kim, *et al.*, “Transient absorption of warm dense matter created by an x-ray free-electron laser,” *Nature Physics* **20**, 1564–1569 (2024).
 - ¹⁸ B. I. Cho, K. Engelhorn, A. A. Correa, T. Ogitsu, C. P. Weber, H. J. Lee, J. Feng, P. A. Ni, Y. Ping, A. J. Nelson, D. Prendergast, R. W. Lee, R. W. Falcone, and P. A. Heimann, “Electronic structure of warm dense copper studied by ultrafast x-ray absorption spectroscopy,” *Phys. Rev. Lett.* **106**, 167601 (2011).
 - ¹⁹ Tun S. Tan, J. J. Kas, and J. J. Rehr, “Real-space green’s function approach for x-ray spectra at high temperature,” *Phys. Rev. B* **104**, 035144 (2021).
 - ²⁰ G. F. Bertsch, “Double gamma decay in light nuclei,” *Part. Nucl.* **4**, 237–243 (1972).
 - ²¹ D. J. Higley, A.H. Reid, Z. Chen, L. L. Guyader, O. Hellwig, A. A. Lutman, T. Liu, P. Shafer, T. Chase, G. L. Dakovski, A. Mitra, E. Yuan, J. Schlappa, H. A. Dürr, W. F. Schlotter, and J. Stöhr, “Femtosecond x-ray induced changes of the electronic and magnetic response of solids from electron redistribution,” *Nat. Comm.* **10**, 5289 (2019).
 - ²² Davide Sangalli, Stefano Dal Conte, Cristian Manzoni, Giulio Cerullo, and Andrea Marini, “Nonequilibrium optical properties in semiconductors from first principles: A combined theoretical and experimental study of bulk silicon,” *Phys. Rev. B* **93**, 195205 (2016).
 - ²³ J Aleksi Soinen, AL Ankudinov, and JJ Rehr, “Inelastic scattering from core electrons: A multiple scattering approach,” *Phys. Rev. B* **72**, 045136 (2005).
 - ²⁴ H. Ebert, J. Stöhr, S. S. P. Parkin, M. Samant, and A. Nilsson, “L-edge x-ray absorption in fcc and bcc Cu metal: Comparison of experimental and first-principles theoretical results,” *Phys. Rev. B* **53**, 16067–16073 (1996).
 - ²⁵ L. Campbell, L. Hedin, J. J. Rehr, and W. Bardyszewski, “Interference between extrinsic and intrinsic losses in x-ray absorption fine structure,” *Phys. Rev. B* **65**, 064107 (2002).

Appendix A: TPA Transition Matrix Elements

The single particle matrix elements are derived by assuming the many-body states are all single Slater determinants. This ignores relaxation of the passive $N - 1$ orbitals. Following Guo,¹⁵ we define the intermediate and final many-body states as particle-hole states with $|F\rangle = a_j^\dagger a_i |I\rangle$. There are two types of intermediate states in TPA: 1) those with a hole in a core-state i and a particle in an arbitrary unoccupied state j , and 2) those with a hole in an arbitrary occupied state a and a particle in state f . These intermediate states are given by $|X\rangle = a_j^\dagger a_i |I\rangle$ and $|X\rangle = a_f^\dagger a_a |I\rangle$. Below we keep this notation with a denoting occupied states, j denoting unoccupied states, and q, r denoting either. In addition, the many-body dipole operator is $D = \sum_{qr} d_{qr} a_q^\dagger a_r$, where

$d_{qr} = \langle q|d|r\rangle$. Noting that the sum in the dipole operator is always collapsed such that the dipole operator connects the ground state to the intermediate state and the intermediate state to the final state, one can rewrite the matrix elements as,

$$\begin{aligned}
M_{IF} &= \sum_j^{unocc} \frac{\langle I|a_i^\dagger a_f d_{fj} a_f^\dagger a_j a_j^\dagger a_i|I\rangle \langle I|a_i^\dagger a_j d_{ji} a_j^\dagger a_i|I\rangle}{\omega + \epsilon_i - \epsilon_j} \\
&+ \sum_a^{occ} \frac{\langle I|a_i^\dagger a_f d_{ai} a_a^\dagger a_i a_f^\dagger a_a|I\rangle \langle I|a_i^\dagger a_f d_{fa} a_f^\dagger a_a|I\rangle}{\omega + \epsilon_a - \epsilon_f} \\
&= \sum_j^{unocc} \frac{d_{fj} d_{ji} \langle I|n_i \bar{n}_f \bar{n}_j|I\rangle \langle I|n_i \bar{n}_j|I\rangle}{\omega + \epsilon_i - \epsilon_j} \\
&- \sum_a^{occ} \frac{d_{ai} d_{fa} \langle I|n_i \bar{n}_f \bar{n}_a|I\rangle \langle I|n_a \bar{n}_f|I\rangle}{\omega + \epsilon_a - \epsilon_f} \\
&= \sum_n^{unocc} \frac{d_{fj} d_{ji}}{\omega + \epsilon_i - \epsilon_j} - \sum_a^{occ} \frac{d_{fa} d_{ai}}{\omega + \epsilon_a - \epsilon_f}, \quad (A1)
\end{aligned}$$

where n, \bar{n} are particle- and hole-number operators respectively. Then using conservation of energy $2\omega = \epsilon_f - \epsilon_i$ gives,

$$\begin{aligned}
M_{IF} &= \sum_j^{unocc} \frac{d_{fj} d_{ji}}{\omega + \epsilon_i - \epsilon_n} + \sum_a^{occ} \frac{d_{fa} d_{ai}}{\omega + \epsilon_i - \epsilon_a} \\
&= \sum_n \frac{d_{fn} d_{ni}}{\omega + \epsilon_i - \epsilon_n}, \quad (A2)
\end{aligned}$$

where the final sum is over all levels n allowed by dipole selection rules. This result for M_{IF} is equivalent to the TPA matrix element M_{if} defined in Eq. (4).